Electronic Supplementary Material (ESI) for Physical Chemistry Chemical Physics.

Supplementary Information for

Probing reaction processes and reversibility in Earth-abundant Na_3FeF_6 for Na-ion batteries

Emily E. Foley,[a,c] Anthony Wong,[b] Rebecca C. Vincent,[a,c] Alexis Manche,[a,c,d] Aryan Zaveri,[c,e] Eliovardo Gonzalez-Correa,[a,c] Gabriel Ménard,[b] Raphaële J. Clément*[a,c]

[a.] *Materials Department, University of California Santa Barbara, California 93106, United States*

[b.] *Department of Chemistry and Biochemistry, University of California Santa Barbara, California 93106, United States*

[c.] *Materials Research Laboratory, University of California Santa Barbara, California 93106, United States*

[d.] *Present address: School of Chemistry, University of St-Andrews, North Haugh, St-Andrews, KY16 9ST, United Kingdom*

[e.] *Physics Department, University of California Santa Barbara, California 93106, United States*

email: rclement@ucsb.edu

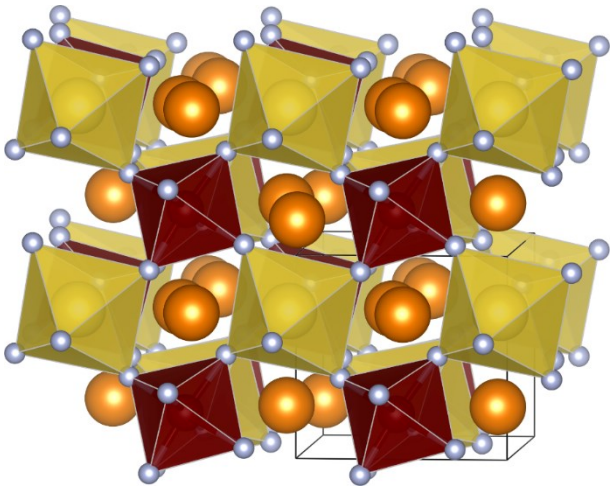

Figure S1, Structure of $Na_3FeF_6 = (Na2)_2(Na1)FeF_6$. The two distinct Na sites, Na1 and Na2, are labeled in yellow and orange, respectively. Fluorine is shown in grey and iron in burgundy.

Table S1, Refined lattice parameters for Na_3FeF_6 and NaF phases in the pristine and ex situ cycled electrode samples.

	Na_3FeF_6						NaF	
	a (Å)	b (Å)	c (Å)	beta	Volume (Å^3)		a (Å)	Volume (Å^3)
Literature[1,2]	5.514	5.734	7.973	90.420	252.078		4.635	99.601
MW Pristine	5.512	5.727	7.962	90.396	251.334		4.633	99.460
MW C-Coated	5.514	5.728	7.964	90.420	251.542		4.632	99.389
BM Pristine	5.514	5.733	7.973	90.414	252.052		4.635	99.595
BM C-Coated	5.514	5.734	7.973	90.420	252.078		4.635	99.601
MW DC 0.65 V	5.514	5.734	7.973	90.420	252.078		4.635	99.601
MW C 4 V	5.513	5.726	7.969	90.430	251.557		4.632	99.390

Supplemental Note 1, Comparing first principles (CRYSTAL17) and experimental NMR parameters

The computed hyperfine (paramagnetic) NMR properties are obtained at 0 K for Na_3FeF_6 supercells containing ferromagnetically-aligned open-shell Fe^{3+} ions. To compare CRYSTAL17 calculation results with experimental data acquired at room temperature, the computed shifts must be subsequently scaled to a value consistent with the paramagnetic state of the system at the temperature of the NMR experiments, using a magnetic scaling factor Φ of the form:

$$\Phi(T_{exp}) = \frac{\langle M(T_{exp}) \rangle}{M_{sat}}, \qquad (1)$$

where M_{sat} is the saturated (ferromagnetic) Fe^{3+} magnetic moment at 0 K, and $\langle M(T_{exp}) \rangle$ the bulk average magnetic moment measured at the sample experimental temperature, T_{exp}. Here, T_{exp} is set to 320 K to account for frictional heating caused by fast (60 kHz) sample rotation during NMR data acquisition.

The magnetic scaling factor in eq. (1) can be evaluated from the experimental magnetic properties of the material:

$$\Phi(T) = \frac{B_0 {\mu_{eff}}^2}{3k_B g_e \mu_B S(T - \Theta)}, \qquad (2)$$

where B_0 is the external magnetic field, μ_{eff} is the effective magnetic moment per Fe site, k_B is Boltzmann's constant, g_e is the free electron g-value, μ_B is the Bohr magneton, S is the formal spin of Fe^{3+} ($3d^5$, $S = 5/2$), and Θ is the Weiss constant. A derivation of eq. (2), starting from the Brillouin function in the low field, high temperature limit, can be found in a previous study by Kim et al.[3] Eq. (2) uses the "spin-only" expression for the magnetic moment and is only strictly valid when the orbital angular momentum is quenched.[4] Yet, for systems where spin-orbit coupling effects are negligible, such as Na_3FeF_6, the spin-only expression is a good approximation to the true magnetic behavior of the system. The experimental inverse magnetic susceptibility vs. temperature curve obtained for Na_3FeF_6 is shown in Figure S2b. From the BM-Na_3FeF_6 data, an effective magnetic moment of 5.85 μ_B per Fe atom and a Weiss temperature of −10 K are obtained. A bulk magnetic scaling factor, Φ, of 0.0328 is obtained for T = 320 K and B_0 = 7.05 T. This value was used to scale the computed ^{23}Na and parameters listed in Tables 1 and S2. The ^{19}F NMR observed chemical shifts were computed to be between 19488 ppm (H20) and 20476 ppm (H35). However, we have previously shown that ^{19}F nuclei directly bonded to paramagnetic centers are too broad and too short lived to be observed[5] and so these signals were not observed.

Table S2: First principles ^{23}Na NMR parameters computed on Na_3FeF_6 H20 and H35 optimized (OPT) structures using the CRYSTAL17 code. The predicted NMR properties have been scaled using a magnetic scaling factor $\Phi = 0.0328$, and are comparable to the room temperature ^{23}Na solid-state NMR data obtained at an external magnetic field of B_0 = 7.05 T. There are two Na local environments in Na_3FeF_6, denoted Na1 and Na2, with multiplicities specified in parentheses in the table below. δ_{iso} is the isotropic Fermi contact shift, $\Delta\delta$ and η are the electron-nuclear dipolar anisotropy and asymmetry parameters, respectively, C_Q is the quadrupolar coupling constant, η_Q is the quadrupolar asymmetry, δ_Q is the second-order quadrupolar shift, and $\delta_{obs} = \delta_{iso} + \delta_Q$ is the observed chemical shift.

Environment	Parameter	OPT H20	OPT H35
Na1 (x1)	δ_{iso}/ppm	2564	1923
	$\Delta\delta$/ppm	369	343
	η	0.5	0.4
	C_Q/MHz	−2.08	−2.13
	η_Q	0.7	0.6
	δ_Q/ppm	−20	−20
	$\delta_{iso} + \delta_Q$/ppm	2544	1903
Na2 (x2)	δ_{iso}/ppm	484	148
	$\Delta\delta$/ppm	−1048	−1106
	η	0.6	0.6
	C_Q/MHz	−2.33	−2.38
	η_Q	0.8	0.8
	δ_Q/ppm	−27	−28
	$\delta_{iso} + \delta_Q$/ppm	457	120

Table S3. Unit cell parameters for the experimental Na_3FeF_6 ($P2_1$) structure,[1] and for the structures optimized using the H20 and H35 functionals in this work.

Structure	*a* / Å	*b* / Å	*c* / Å	α / °	β / °	γ / °
EXP	11.028	11.468	15.946	90.0	90.42	90.0
OPT H20	10.972	11.452	15.875	90.0	90.9	90.0
OPT H35	10.905	11.381	15.777	90.0	90.9	90.0

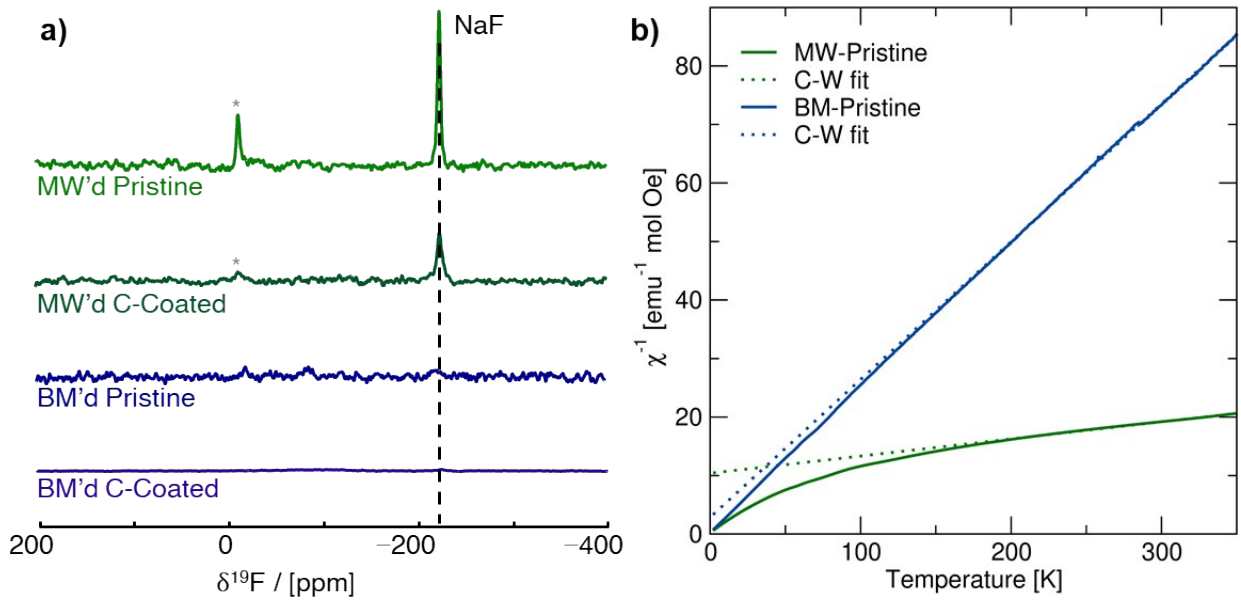

Figure S2, ^{19}F ssNMR and Magnetic Data collected on the As-Prepared Na_3FeF_6 Samples. a) ^{19}F spin echo NMR spectra obtained on the as-prepared materials. Each spectrum is scaled according to the number of moles of material in the rotor and the number of scans collected during the NMR experiment. Spinning sidebands are indicated by an asterisk (*). b) Inverse magnetic susceptibility curves obtained at 2000 Oe on the pure pristine Na_3FeF_6 samples (solid lines), and associated Curie-Weiss fits (dashed lines).

Table S4, Summary of ^{57}Fe Mössbauer parameters for this study and relevant reference materials. All values reported here are referenced to α-Fe at 290 K.

As-Synthesized		
	δ (mm/s)	**ΔE_Q (mm/s)**
MW Pristine	0.27	0.09
MW C-coated	0.27	0.11
BM Pristine	0.27	0.15
BM C-coated	0.27	0.15

Ex Situ		Fe^{3+}			Reduced-Fe		
		δ (mm/s)	**ΔE_Q (mm/s)**	**Signal %**	**δ (mm/s)**	**ΔE_Q (mm/s)**	**Signal %**
MW thick	**DC 1.3 V**	0.27	0.14	91%	1.16	0.19	9%
	DC 0.65 V	0.27	0.14	90%	1.16	0.2	10%
	C 4.0 V	0.28	0.14	95%	1.14	0.28	5%
	2nd DC 0.65 V	0.27	0.14	88%	1.15	0.20	12%
BM thick	**DC 0.65 V**	0.27	0.15	89%	1.17	0.19	11%
	C 4.0 V	0.26	0.14	96%	1.19	0.20	4%
BM thin	**DC 0.65 V**	0.26	0.15	90%	1.14	0.28	10%
	C 4.0 V	0.26	0.14	95%	1.17	0.25	5%

	δ (mm/s)	**ΔE_Q (mm/s)**	**Reference**
$Fe(II)F_2$	1.361	2.791	[6]
$Fe(III)F_3$	0.481	0.05	[7]
$NaFe(II)F_3$	1.25	1.25	[8]
$NaFe(III)F_4$	0.414	0.632	[9]
$Na_2Fe(II)Fe(III)F_7$	1.17	1.49	[9]
	0.402	0.566	
$Na_3Fe(III)F_6$	0.27	0.15	This work

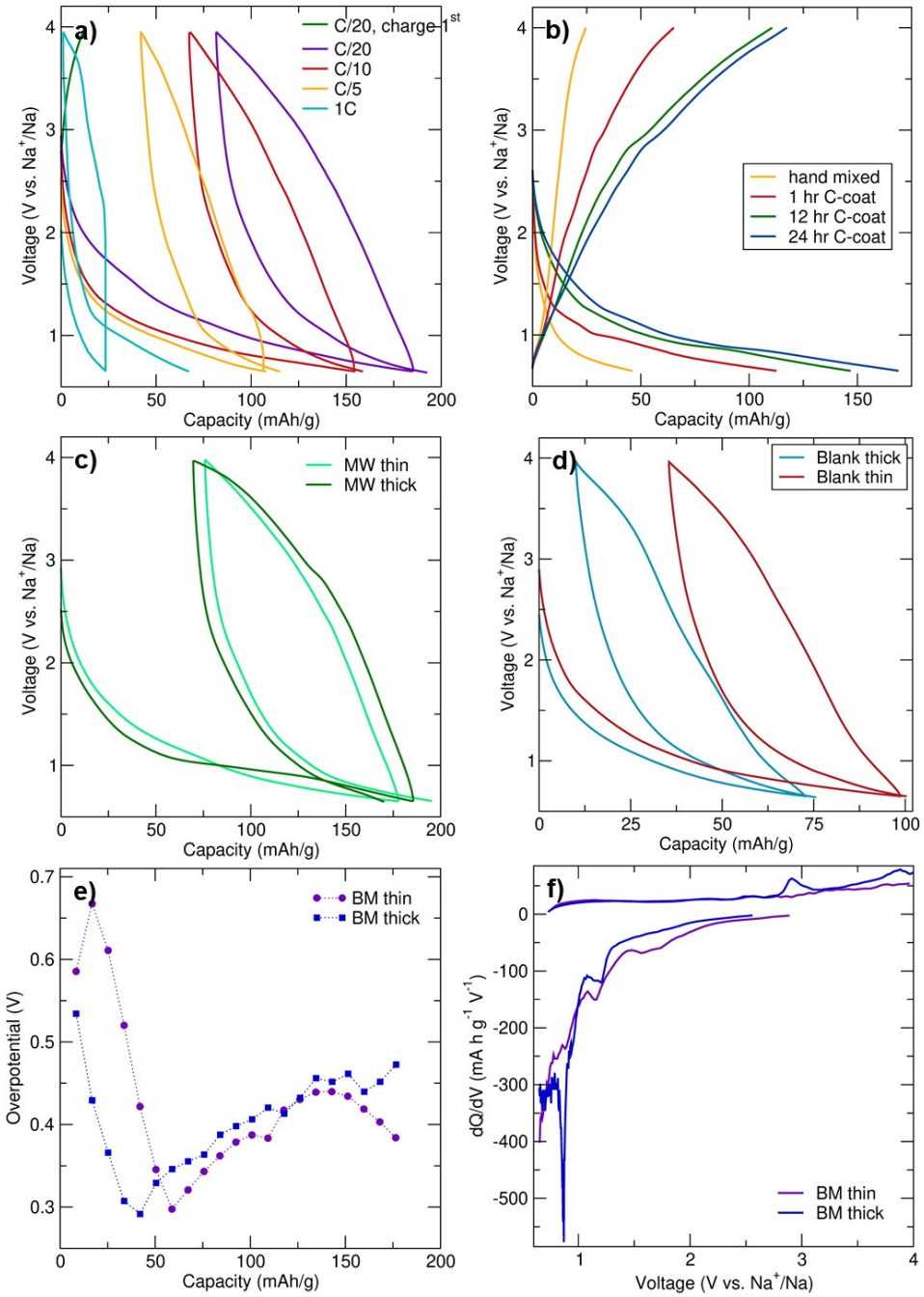

Figure S3, Additional Electrochemical Characterization of Na_3FeF_6. a) Electrochemical profile obtained on BM thin cells when charged first and at various cycling rates. b) 1st discharge-charge electrochemical profiles obtained on BM thick cells hand ground with C for 15 min and C-coated for 1 hr, 12 hr, and 24 hr. c) Electrochemical profiles corresponding to the 1st two discharge-charge cycles and obtained on MW thick and thin cells. d) Electrochemical profiles corresponding to the 1st discharge-charge cycle obtained on the thick and thin blank (NaF) cells. e) Overpotential measured by GITT at various points during the first discharge process. f) dQ/dV comparison for the 1st discharge-charge cycle for BM thin and thick cells.

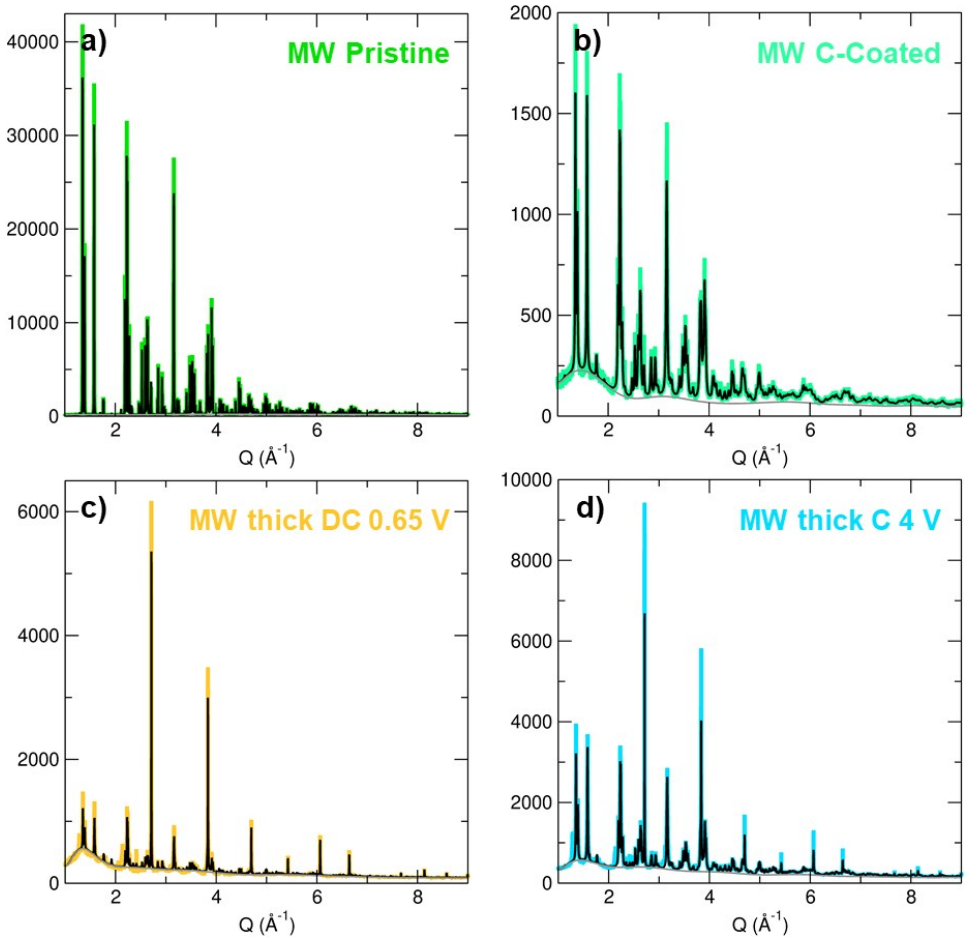

Figure S4, Synchrotron XRD ex situ Characterization. Synchrotron XRD pattern (colored line) and the total Rietveld refinement (black) for MW pristine (a), MW C-coated (b), and MW thick discharge (c) and charge (d). The grey line corresponds to the background used for each diffraction pattern which is predominantly attributed to the Kapton capillary used to hold each sample.

Table S5, Summary of attempted phases used to fit the unidentified reflections at Q ≈ 1.3, 1.9, 2.1, 2.4, 3.1, and 3.8 $Å^{-1}$ in the *ex situ* SXRD patterns. All of the phases containing H_2O were also attempted dehydrated.

Formula	Space Group
Fe	*Fm*−3*m, Im*−3*m*
FeF_2	$P4_2/mnm$
$Fe_2F_5(OH)(H_2O)$	*Fd*−2*mZ*
$FeF_2(H_2O)_4$	*R*−3*mH*
FeF_3	*R*−3*c, Fd*−3*m, R*−3*c, P*321*, Cmcm, Pm*−3*m*
FeOF	$P4_2/mnm$
FeO	*Fm*−3*m, R*−3*m*
Fe_3O_4	*Cmcm, Cc, F*−43*m, Fd*−3*m*
Fe_2O_3	*Aea*2*, Cmcm*
Fe(OH)F	*Pnma*
$FeF_2(H_2O)_4$	*R*−3*m*
$Fe_3F_8(H_20)_2$	*C*2/*m*
$FeF_{2.5}(H_2O)_{0.5}$	*Fd*−3*m*
$Fe_2F_5(H_2O)_2$	*Imma*
$FeF_3(H_2O)_{0.33}$	*Cmcm*
$FeF_3(H_2O)3$	*P*4/*n*
$NaFeF_3$	*Cmcm, Pnma*
$Na_2Fe_2F_7$	*C*2/*c*
Na_3FeF_6	$P2_1$
$NaFeF_4$	$P2_1/c$
$Na_5Fe_3F_{14}$	$P2_1/c$, $P4_22_12$

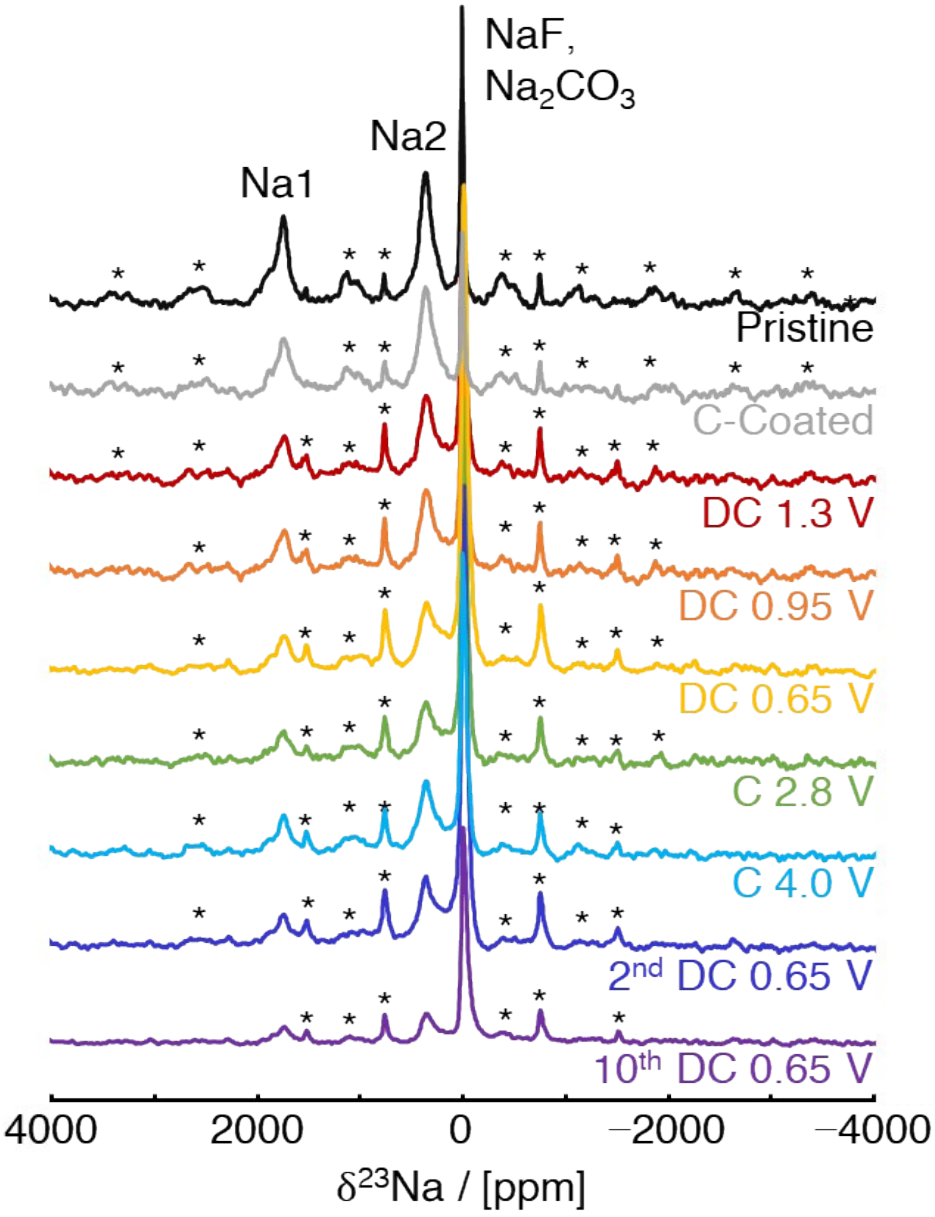

Figure S5, Expanded ^{23}Na NMR ex situ Characterization. ^{23}Na spin echo NMR spectra obtained on MW thick Na_3FeF_6 at various stages of charge. Each spectrum has been scaled according to the number of moles of material in the rotor and the number of scans collected during the NMR experiment. Spinning sidebands are indicated by an asterisk (*).

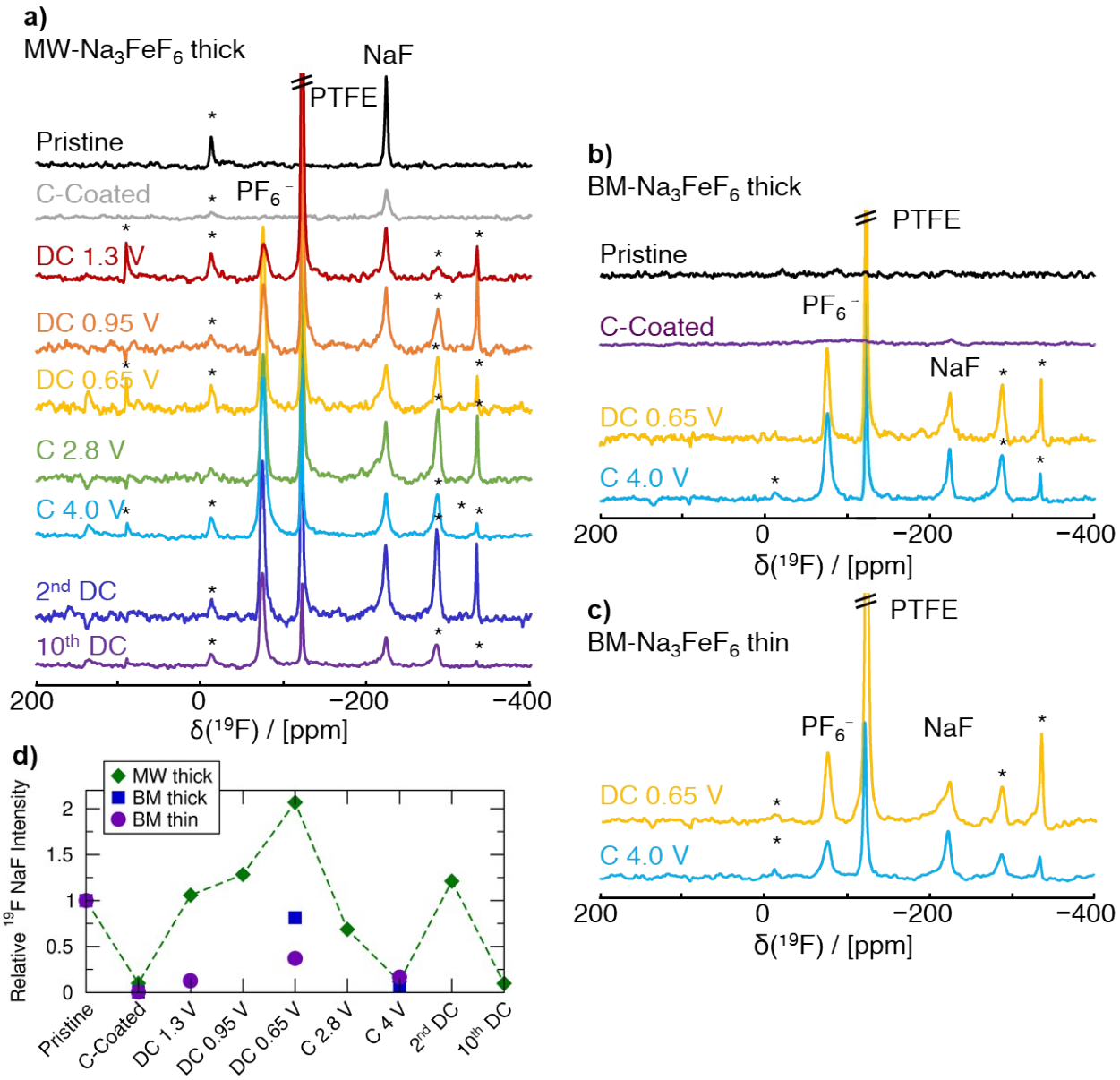

Figure S6, ^{19}F NMR ex situ Characterization. ^{19}F spin echo NMR spectra collected on *ex situ* MW thick (a), BM thick (b), and BM thin (c) Na_3FeF_6. Each spectrum has been scaled according to the number of moles of material in the rotor and the number of scans collected during the NMR experiment. Spinning sidebands are indicated by an asterisk (*). d) Relative intensity of the ^{19}F NMR signal (± 0.1) corresponding to a diamagnetic NaF phase in *ex situ* samples stopped at various states of charge.

Table S6, Summary of Observed Conversion by ^{23}Na NMR Compared to the Electrochemical Capacity. Summary of ^{23}Na NMR *ex situ* characterization of conversion products and the expected capacity if conversion occurs through Reaction Path A (Fe^0) or B (Fe^{2+}). The observed capacity at each point for the different cells are shown in the last column.

	^{23}Na NMR Characterization						**Observed Capacity (mAh/g)**
	Phase mol % (± 5%)		**Phase mol % (± 5%) adjusted by initial NaF**		**Expected Capacity (mAh/g) for Each Reaction Path**		
	Na_3FeF_6	**NaF**	**Na_3FeF_6**	**NaF**	**A (Fe^0)**	**B (Fe^{2+})**	
MW thick							
Pristine	84%	16%	--	--	--	--	--
C-coated	80%	20%	--	--	--	--	--
DC 1.3 V	47%	53%	58%	42%	36	17	16
DC 0.65 V	31%	69%	39%	61%	70	32	100
C 4 V	44%	56%	53%	47%	43	20	29
BM thick							
Pristine	99%	1%	--	--	--	--	--
C-coated	97%	3%	--	--	--	--	--
DC 0.65 V	37%	63%	38%	62%	73	33	87
C 4 V	58%	42%	59%	41%	34	16	31
BM thin							
DC 1.3 V	77%	23%	91%	9%	3	6	17
DC 0.65 V	43%	57%	44%	56%	58	27	81
C 4 V	70%	30%	72%	28%	21	10	38

Supplemental Note 2, Identification of Oxidation State of "Reduced-Fe" Species Present in ex situ BM Thin Discharged Samples

The "reduced-Fe" species observed via ^{57}Fe Mössbauer may correspond to a surface-component of superparamagnetic Fe^0 nanoparticles,[10] as would be expected from the previously proposed reaction mechanism for Na_3FeF_6.[11] Alternatively, the "reduced-Fe" signal has an isomer shift similar to high spin Fe^{2+} species, such as in FeF_2 (δ = 1.36 mm/s, ΔE_Q = 2.79 mm/s)[12], but with a much smaller ΔE_Q. This small ΔE_Q indicates a more isotropic charge density around the Fe^{2+} species as compared to FeF_2, *e.g.*, due to fast electron hopping between Fe species on the timescale of the Mössbauer experiments, as in a mixed valent Fe^{2+}/Fe^{3+} phase [13,14]. To differentiate between the presence of Fe^{2+} species or Fe^0 nanoparticles, XPS and magnetometry measurements were carried out on *ex situ* BM thin samples.

XPS spectra shown in Figure S7a were fitted with one peak to the Fe^{3+} $2p_{3/2}$ state and one peak to the Fe^{2+} $2p_{3/2}$ state at 715 eV and 711 eV binding energy (BE), respectively, similarly to fits on Li_3FeF_6 reported elsewhere.[15] At higher BE within the Fe $2p_{3/2}$ envelope, another peak is ascribed to surface structures and/or a Fe^{2+} satellite peak.[16] The pristine XPS spectrum features both Fe^{3+} and Fe^{2+} due to the reduction of surface Fe^{2+} species induced by the high-energy milling synthesis technique. As the *ex situ* samples were carbon-coated and mixed with a polymeric binder, their overall intensity is decreased compared to the pristine material. The *ex situ* sample obtained upon 0.65 V discharge exhibits an increased Fe^{2+} to Fe^{3+} signal ratio which decreases slightly in the sample obtained on subsequent charge to 4 V, suggesting the presence of Fe^{2+} species in the discharged sample, with minimal reversibility on charge. Fe^0 $2p_{3/2}$ (707 eV BE) and $2p_{1/2}$ (720 eV BE) signals are not observed but the overlapping of F 1*s* plasmon loss peaks near the Fe 2*p* envelope may obscure this signal if Fe^0 is present in small amounts. Thus, these results suggest that Fe^{2+} is present rather than Fe^0, at least at the surface of the particles.

Magnetic hysteresis curves at 2K (Figure 5b) for the BM thin pristine and 0.65 V discharged samples show characteristic paramagnetic behavior, reaching a saturation magnetization (M_s) at high fields proportional to the number of unpaired electrons on each magnetic ion (μ_B/Fe). The M_s decreases in the discharged sample (3.34 μ_B/Fe) compared to the pristine (4.61 μ_B/Fe) in line with the formation of Fe^{2+} on discharge from Fe^{3+} (5 μ_B/Fe^{3+}, 4 μ_B/Fe^{2+}), with slightly smaller M_s values obtained than theoretically predicted due to the weak antiferromagnetic interactions present in Na_3FeF_6 as discussed earlier. Magnetic susceptibility data (Figure S6) are consistent with these results, and μ_{eff} values obtained from Curie-Weiss fits are equal to 5.80 μ_B and 5.05 μ_B per Fe atom for the pristine and 0.65 V discharged Na_3FeF_6 samples, respectively. Thus, these results along with our previous XPS and ^{57}Fe Mössbauer results, indicate that this "reduced-Fe" species is an amorphous Fe^{2+}-containing phase that may possibly also contain Fe^{3+} species.

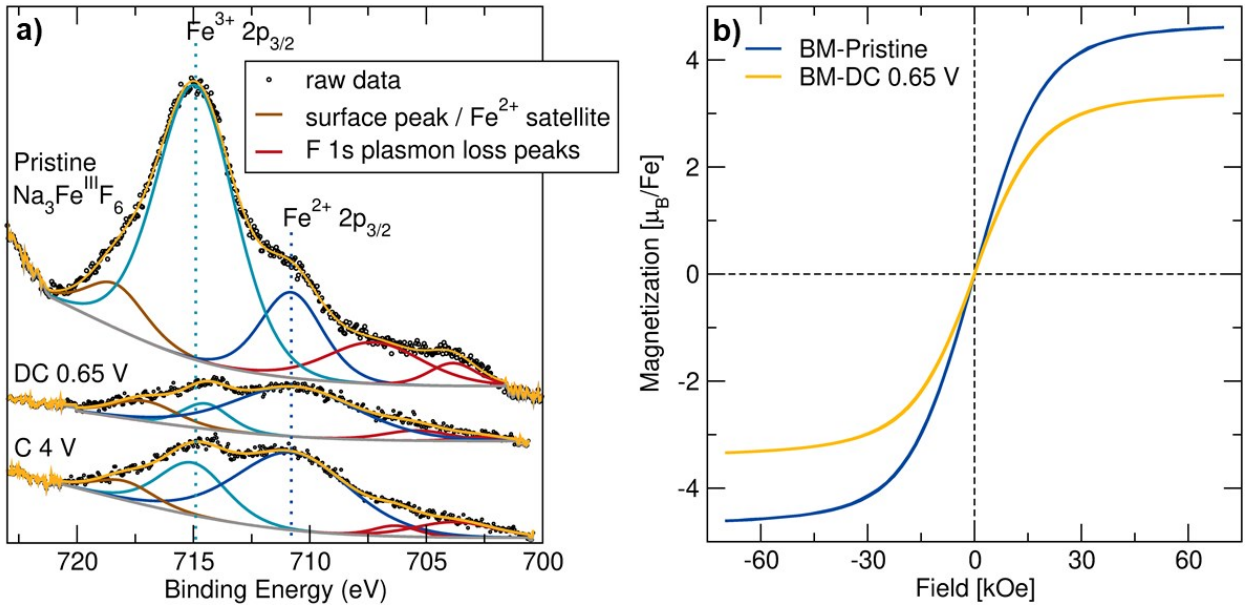

Figure S7, XPS and Magnetometry of ex situ BM thin Na_3FeF_6. a) XPS spectra (black dots) with corresponding fits (yellow) for BM pristine Na_3FeF_6 and for thin discharged and charged *ex situ* electrodes show an increase in Fe^{2+} (dark blue) upon discharge compared to Fe^{3+} (cyan). b) Magnetization vs. field measurements for BM pristine Na_3FeF_6 and for thin *ex situ* discharged electrodes at 2 K showing an overall decrease of magnetization for the discharged sample.

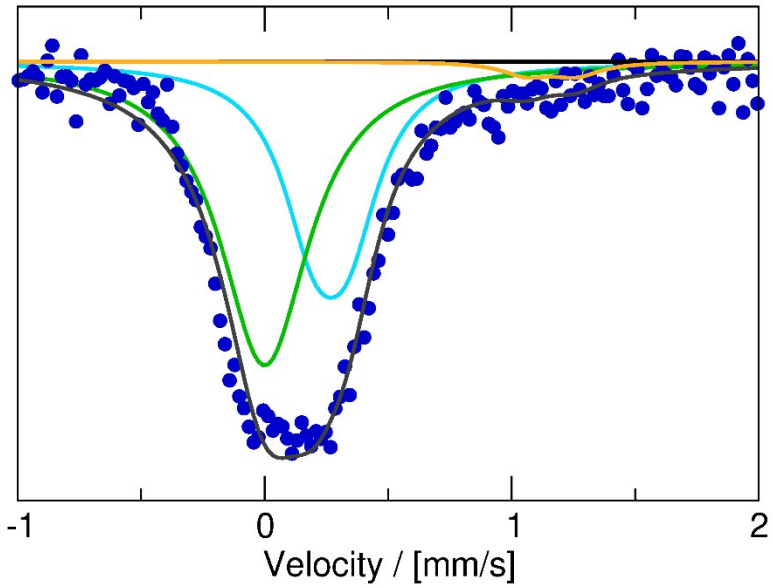

Figure S8, ^{57}Fe Mössbauer of Chemically Reduced BM-Na_3FeF_6. ^{57}Fe Mössbauer spectra for chemically reduced BM-Na_3FeF_6 fitted with 58% bulk Fe^0 (δ = 0 mm/s, green), 39% O_h-Fe^{3+} in Na_3FeF_6 (δ = 0.27 mm/s, cyan), and 3% Fe^{2+} ($\delta \approx 1.16$ mm/s and $\Delta E_Q \approx 0.2$ mm/s, orange) similar to that seen in the *ex situ* samples.

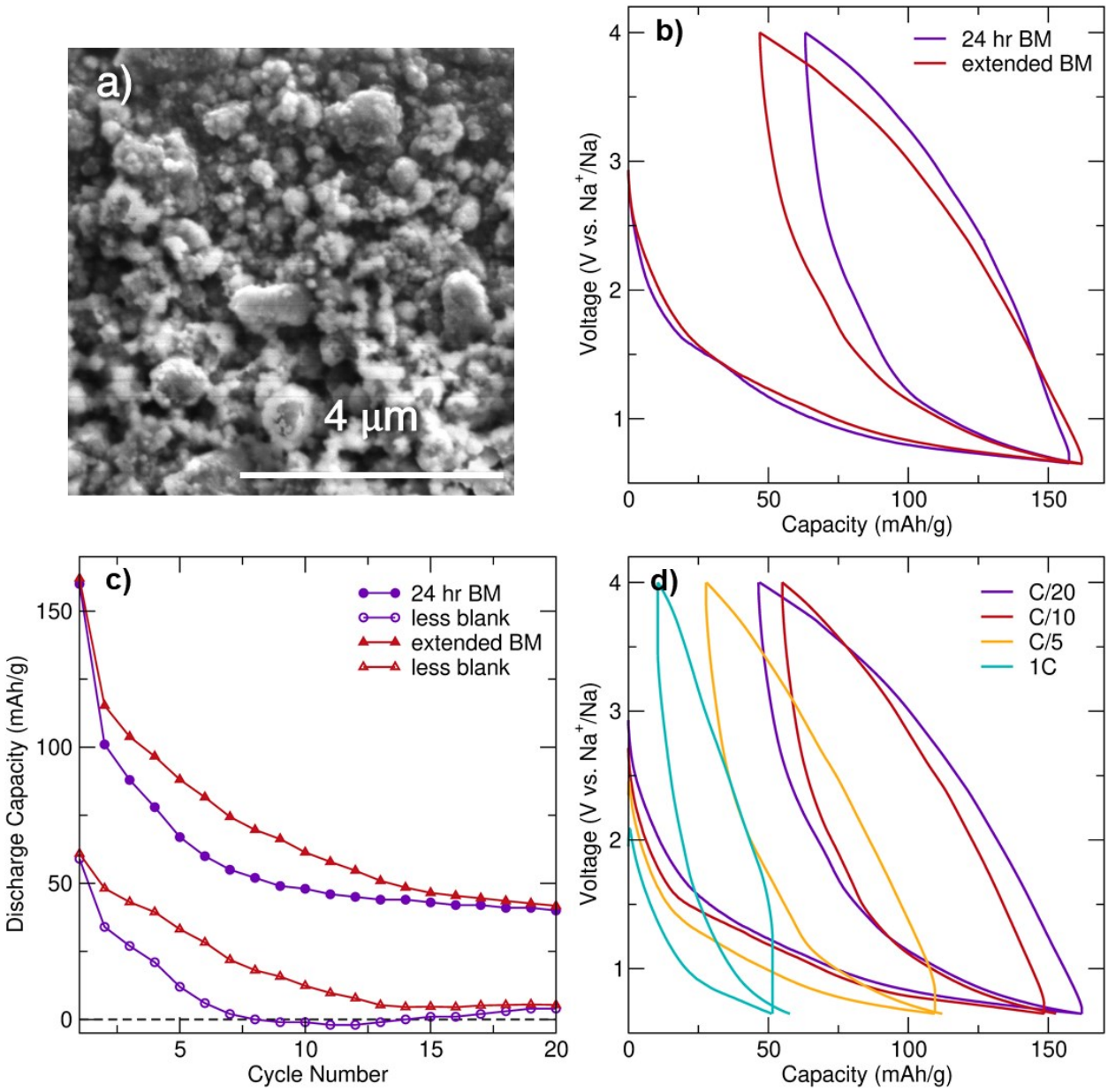

Figure S9, SEM and Electrochemical Testing of Particle Size Reduction of BM-Na_3FeF_6. Particle size reduction of BM-Na_3FeF_6 was completed by adding an additional 12 hr ball-milling step with five 10 mm and ten 5 mm ZrO_2 balls following the previous 24 hr ball-milling step. a) SEM images of the extended BM-Na_3FeF_6 particles. 24 hr BM C-Coating and extended C-coating BM-Na_3FeF_6 thin cells comparison of their b) first two charge and discharge cycles (C/20 rate) and c) discharge capacity retention for Na_3FeF_6 cells (filled symbols) and for Na_3FeF_6 cells with the corresponding blank cell capacity subtracted (unfilled symbols). d) First two charge and discharge cycles for the extended BM-Na_3FeF_6 thin cells at various rates.

References

1 E. N. Matvienko, O. V. Yakubovich, M. A. Simonov, A. N. Ivashchenko, O. K. Mel'nikov and N. V. Belov, The crystal structure of the synthetic Fe-cryolite Na3FeF6, *Dokl. Akad. Nauk SSSR*, 1981, **257**, 105–108.

2 Y. Shirako, Y. G. Shi, A. Aimi, D. Mori, H. Kojitani, K. Yamaura, Y. Inaguma and M. Akaogi, High-pressure stability relations, crystal structures, and physical properties of perovskite and post-perovskite of NaNiF3, *J. Solid State Chem.*, 2012, **191**, 167–174.

3 J. Kim, D. S. Middlemiss, N. A. Chernova, B. Y. X. Zhu, C. Masquelier and C. P. Grey, Linking local environments and hyperfine shifts: A combined experimental and theoretical 31P and 7Li solid-state NMR study of paramagnetic Fe(III) phosphates, *J. Am. Chem. Soc.*, 2010, **132**, 16825–16840.

4 C. Delmas, D. Carlier, G. Ceder, M. Ménétrier and C. P. Grey, Understanding the NMR shifts in paramagnetic transition metal oxides using density functional theory calculations, *Phys. Rev. B*, 2003, **67**, 174103.

5 R. J. Clément, D. Kitchaev, J. Lee and Gerbrand Ceder, Short-Range Order and Unusual Modes of Nickel Redox in a Fluorine-Substituted Disordered Rocksalt Oxide Lithium-Ion Cathode, *Chem. Mater.*, 2018, **30**, 6945–6956.

6 L. R. Walker, G. K. Wertheim and V. Jaccarino, Interpretation of the 57Fe Isomer Shift, *Phys. Rev. Lett.*, 1961, **6**, 98–101.

7 G. K. Wertheim, H. J. Guggenheim and D. N. E. Buchanan, Sublattice magnetization in FeF3 near the critical point, *Phys. Rev.*, 1968, **169**, 465–470.

8 I. D. Gocheva, M. Nishijima, T. Doi, S. Okada, J. ichi Yamaki and T. Nishida, Mechanochemical synthesis of NaMF3 (M = Fe, Mn, Ni) and their electrochemical properties as positive electrode materials for sodium batteries, *J. Power Sources*, 2009, **187**, 247–252.

9 U. K. Dey, N. Barman, S. Ghosh, S. Sarkar, S. C. Peter and P. Senguttuvan, Topochemical Bottom-Up Synthesis of 2D- and 3D-Sodium Iron Fluoride Frameworks, *Chem. Mater.*, 2019, **31**, 295–299.

10 P. Liao, B. L. MacDonald, R. A. Dunlap and J. R. Dahn, Combinatorially prepared [LiF]1-xFex nanocomposites for positive electrode materials in li-ion batteries, *Chem. Mater.*, 2008, **20**, 454–461.

11 R. A. Shakoor, S. Y. Lim, H. Kim, K. W. Nam, J. K. Kang, K. Kang and J. W. Choi, Mechanochemical synthesis and electrochemical behavior of Na3FeF6 in sodium and lithium batteries, *Solid State Ionics*, 2012, **218**, 35–40.

12 G. K. Wertheim and D. N. E. Buchanan, Temperature dependence of the Fe57 hfs in FeF2 below the Néel temperature, *Phys. Rev.*, 1967, **161**, 478–482.

13 R. N. Panda, N. S. Gajbhiye and G. Balaji, Magnetic properties of interacting single domain Fe3O4 particles, *J. Alloys Compd.*, 2001, **326**, 50–53.

14 P. Gütlich, Fifty years of Mössbauer spectroscopy in solid state research - Remarkable achievements, future perspectives, *Z. Anorg. Allg. Chem.*, 2012, **638**, 15–43.

15 A. Basa, S. Wojtulewski, B. Kalska-Szostko, M. Perkowski, E. Gonzalo, O. Chernyayeva, A. Kuhn and F. García-Alvarado, Carbon coating of air-sensitive insulating transition metal fluorides: An example study on α-Li3FeF6 high-performance cathode for lithium ion batteries, *J. Mater. Sci. Technol.*, 2020, **55**, 107–115.

16 A. P. Grosvenor, B. A. Kobe, M. C. Biesinger and N. S. McIntyre, Investigation of multiplet splitting of Fe 2p XPS spectra and bonding in iron compounds, *Surf. Interface Anal.*, 2004, **36**, 1564–1574.